Astron. Nachr. / AN **327**, No. 2/3, 227–230 (2006) / **DOI** 10.1002/asna.200510512

The X-ray and radio jets of quasars on kiloparsec scales

S.G. JORSTAD and A.P. MARSCHER

Institute for Astrophysical Research, Boston University, 725 Commonwealth Ave., Boston, MA 02215, USA

Received 10 October 2005; accepted 15 November 2005; published online 20 February 2006

Abstract. We have observed five quasars (0827+243, 0923+392, 1222+216, 1317+520, and 2209+080) with Chandra at 0.2-8 keV and with the VLA at 5 and 15 GHz. The X-ray emission is detected from all the radio jets except for 0923+392, whose double radio jet only extends out to the edge of the X-ray PSF. We model the spectral energy distribution of the jet features assuming that the X-ray emission originates via inverse Compton scattering off the cosmic microwave background by relativistic electrons. For two sources (0827+243 and 1222+216) proper motion on parsec scales is consistent with the Doppler factors derived from the model, which implies that no deceleration occurs between parsec and kiloparsec jets.

Key words: galaxies: jets – quasars: individual (0827+243, 0923+392, 1222+216, 1317+520, and 2209+080)

1. Introduction

The discovery of luminous X-ray jets in quasars by Chandra (e.g., Schwartz et al. 2000) is among the most significant results in the astrophysics of active galactic nuclei over the past 10 years. Searches for X-ray jets in quasars indicate that the probability of detecting the extended X-ray emission from quasars with kiloparsec-scale radio jets is about 60% (10/17 in Sambruna et al. 2004, 12/20 in Marshall et al. 2005). All these X-ray jets are one-sided and their morphology varies from long straight jets to jets bent by up to 90°. In the majority of the quasars bright X-ray features track bright radio knots. These knots have flat X-ray spectral indices ($\alpha_{\rm x} \sim 0.4$–0.6, $S_\nu \propto \nu^{-\alpha}$) and "normal" radio spectral indices ($\alpha_{\rm r} \sim 0.7$–0.8). In some sources the spectrum changes along the jet, with the ratio of X-ray to radio intensity declining with distance from the core. The latter are quasars with high apparent speed on pc-scales: 3C 273 (Marshall et al. 2001), PKS 1127−145 (Siemiginowska et al. 2002), and 0827+243 (Jorstad & Marscher 2004).

Analysis of the spectral energy distributions (SEDs) (Sambruna et al. 2004; Marshall et al. 2005) suggests that Fanaroff-Riley class II (FR II) X-ray jets can be interpreted as inverse Compton scattering off the cosmic microwave background by relativistic electrons (IC/CMB; Tavecchio et al. 2000; Celotti et al. 2001). This requires that the jet be aligned closely to the line of sight and possess a bulk Lorentz factor $\geq$10 (e.g., Marshall et al. 2005). Possible alternative models for X-ray production in large-scale jets explain the SEDs as pure synchrotron emission from either a single (Dermer & Atoyan 2002) or dual (Jester et al. 2005) population of relativistic electrons. The physics of relativistic jets in FR II sources is an important aspect of energy transport and dissipation between the nucleus and lobes and of regulation of the temperature and morphology of galaxy clusters in the universe (McNamara et al. 2005). The major issue is whether the Lorentz factor Γ of the jet remains high out to the hotspot, declines gradually owing to interaction with the ambient external medium or backflow, or decreases abruptly at bends, where it presumably deflects through an encounter with the external medium.

Correspondence to: jorstad@bu.edu

2. Observations and data reduction

We observed the quasars for 18 ks with the ACIS-S detector of the Chandra X-Ray Observatory during Cycle 3. We used version 3.0.2 of the CIAO software and version 2.26 of the CALDB calibration database and followed the threads provided in http://cxc.harvard.edu/ciao/threads for the data analysis. We performed observations with the Very Large Array (VLA) of the National Radio Astronomy Observatory (NRAO) at 15 GHz in B array on 2002 August 19, and at 5 GHz in A array on 2003 August 28. The data were edited and calibrated using the Astronomical Image Processing System (AIPS) software provided by NRAO. The resulting X-ray and radio images are shown in Figure 1 where the main jet features detected at X-ray and radio wavelengths are indicated. A field containing 0827+243 was observed with the

Wide Field Planetary Camera 2 of the Hubble Space Telescope (HST) at $\lambda_{\rm eff} = 708.14$ nm. We retrieved the images of this field from the HST archive and estimated a 1σ upper limit for the flux of the optical jet of this quasar of 2.5×10^{-30} erg cm^{-2} s^{-1} Hz^{-1} (see Jorstad & Marscher 2004).

3. The X-ray emission in the large-scale jets

In the γ-ray blazar 0827+243 the radio jet does not even become detectable until the X-ray jet first extends up to $5''$ from the nucleus and then executes an apparent bend of about $\sim 90^\circ$ before extending another $2''$. The quasars 1222+216, 1317+520 and 2209+080 have extended, multicomponent radio structure (see Fig. 1). The quasar 1222+216, which is also a γ-ray blazar, possesses a strong bend of the radio jet at $\sim2''$ from the core. The X-ray emission is seen only within the inner radio jet region before and at the bend. In the quasars 1317+520 and 2209+080 the X-ray jet features coincide with bright radio knots located in the apparently straight part of the radio jets.

We have found (Jorstad & Marscher 2004) that the SEDs of the jet features in the quasar 0827+243, for which measurements in the optical regions are available, are approximated very well by the IC/CMB X-ray model combined with synchrotron radio emission. We use the same approach with the formalism described in the Appendix of Jorstad & Marscher (2004) to estimate the jet parameters of the other quasars, although we stress that this interpretation is not unique, especially for the SEDs of the jet features limited by the radio and X-ray regions only. Figure 2 shows the observed and model SEDs of the most prominent features in the jets. Table 1 gives the physical parameters used for the calculations: z is the redshift, α is the radio spectral index (except the knot C2 in 0827+243, for which the X-ray spectral index is applied), B is the strength of the magnetic field, and δ is the Doppler factor. In the case of of the quasar 0827+243 the optical upper limit for knots C2 and C4 restricts the energy distribution of the relativistic electrons since $\gamma_{\rm max}$ should not be higher than 5×10^5 and $\gamma_{\rm min}$ should not be lower than 15, otherwise the knots have to be detected at optical wavelengths ($\gamma_{\rm max}$ and $\gamma_{\rm min}$ are maximum and minimum electron Lorentz factors, respectively). In the calculations the indicated values of the energy cutoffs of the relativistic electron population have been adopted for all quasars along with the assumption of an electron-proton plasma in the jet. These parameters of the jet features are used to estimate the kinetic luminosities of the X-ray-emitting knots (column $L_{\rm kin}$ of Table 1). We apply an inhomogeneous Friedmann-Lemaitre-Robertson-Walker cosmology with $\Omega_{\rm m} = 0.3$, $\Omega_\Lambda = 0.7$, and Hubble constant $H_0 = 70$ km s^{-1} Mpc^{-1}.

4. Discussion

Although the SEDs of the jet features in the quasars 1222+216, 1317+520, and 2209+080 can be explained by synchrotron radiation from a single population of relativistic electrons, the SED of feature C4 of the quasar 0827+243

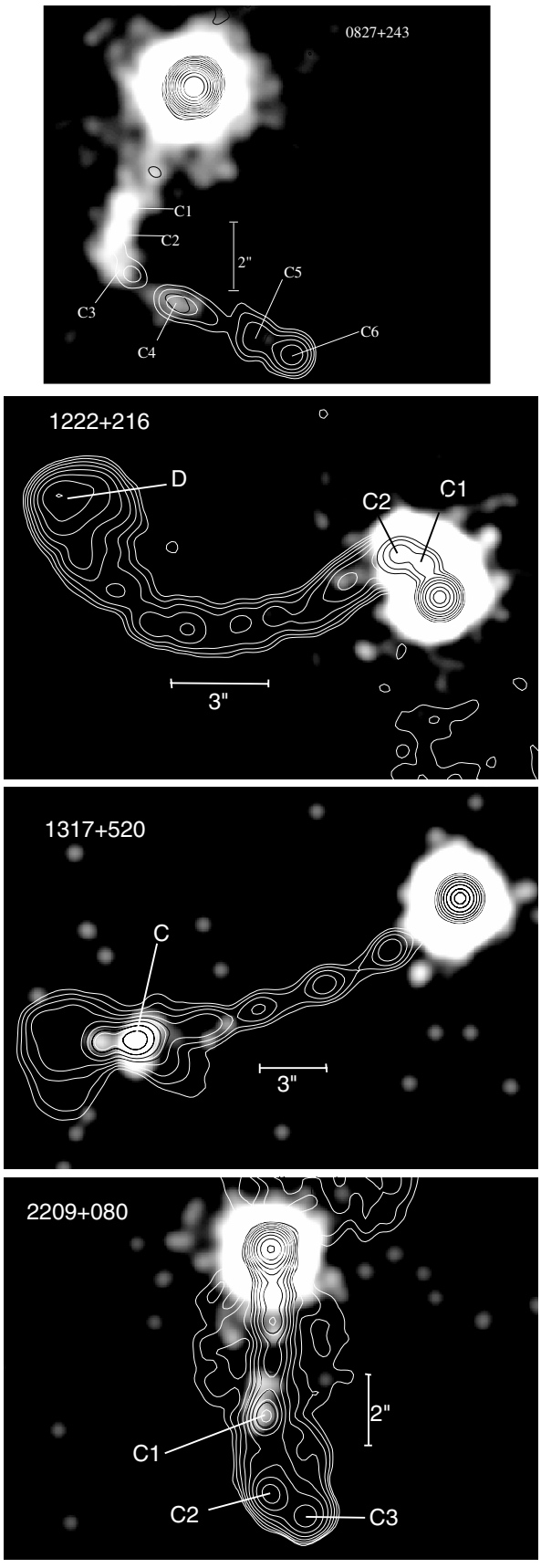

Fig. 1. Chandra (white/gray scale) and VLA 5 GHz (contours) images of the quasars. Contours are in factors of 2 of the peak intensity of 1.36 Jy/beam (0827+243), 0.93 Jy/beam (1222+216), 0.39 Jy/beam (1317+520), and 0.65 Jy/beam (2209+080). The images are convolved with a beam of FWHM 0.5×0.5 arcsec^2.

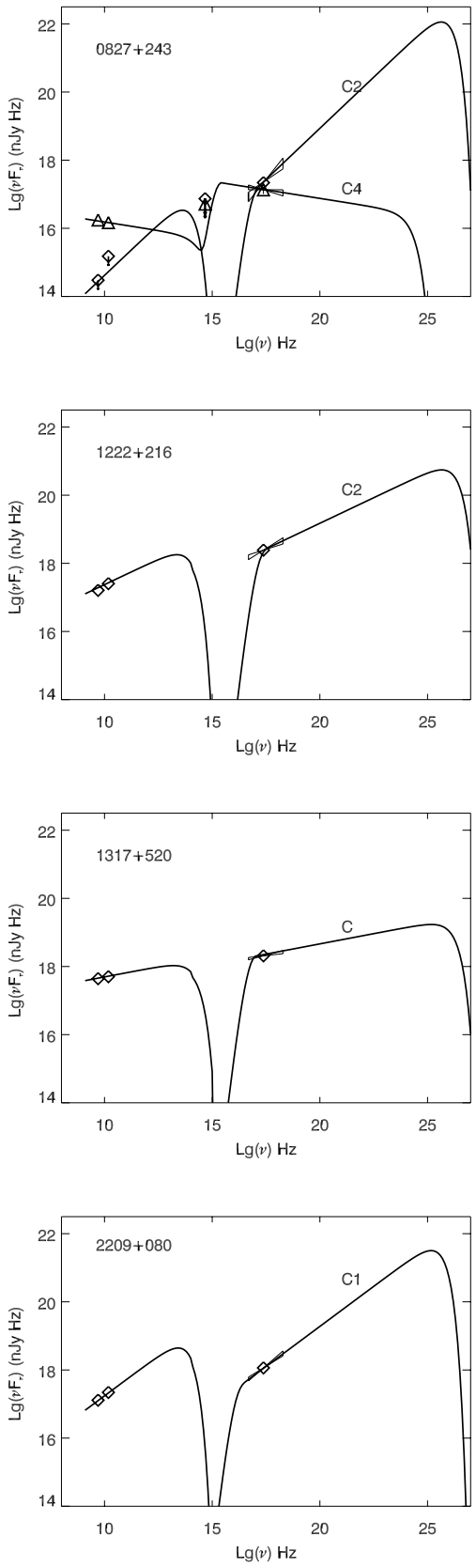

Fig. 2. The observed spectral energy distribution for jet knots (triangles/diamonds). The solid curves show the simulated SEDs for combined synchrotron and CMB/IC emission of a single population of relativistic electrons with $\gamma_{\rm min} = 15$ and $\gamma_{\rm max} = 5 \times 10^5$. The parameters used to compute the SEDs are given in Table 1.

Table 1. Physical parameters of jets.

Source	z	Comp.	α	B (μG)	δ	$L_{\rm kin}$ (erg s^{-1})
0827+243	0.939	C2	0.4±0.2	2	24	1×10^{45}
		C4	1.1±0.1	60	3.3	6×10^{47}
1222+216	0.435	C2	0.7±0.1	12	17	9×10^{45}
1317+520	1.06	C	0.88±0.05	49	10	9×10^{46}
2209+080	0.485	C1	0.53±0.08	30	5	5×10^{45}

does not allow such a possibility. A model with two different populations of relativistic electron cannot be ruled out for any quasar. These models require a population of relativistic electrons with $\gamma_{\rm max} \sim 5 \times 10^7$ located hundreds of kiloparces from the nucleus. The IC/CMB model combined with synchrotron radio emission can easily explain the observed SEDs with reasonable energy cutoffs of the relativistic electron distribution. Another striking property of the IC/CMB model is that the Doppler factors of X-ray feature C2 in the quasar 0827+243 and knot C2 in the quasar 1222+216 coincide with the estimated parsec-scale δ based on the apparent speed (there are no published estimates of apparent speed for the quasars 1317+520 and 2209+080). A widely used method to estimate the Doppler factor from VLBI data assumes that the highest apparent speed detected in a source defines the lowest possible Lorentz factor of the jet, $\Gamma \geq (1+\beta_{\rm app}^2)^{-1/2}$. The viewing angle is then taken to be $\Theta_\circ \leq \sin^{-1}(1/\beta_{\rm app})$, leading to $\delta \sim \beta_{\rm app}$. Different measurements of the apparent speed in the quasar 0827+243 give similar values of the apparent speed, $\beta_{\rm app} = (22 \pm 2)c$ (Jorstad et al. 2001) and $\beta_{\rm app} = (26 \pm 4)c$ (Piner et al. 2004), which produces a Doppler factor consistent with δ derived on kiloparsec scales. Moreover, the X-ray and parsec-scale radio jets lie in the same direction (see Fig. 3), so there is no evidence of bending that would change the angle between the jet axis and the line of sight. This strongly implies that the bulk Lorentz factor remains constant from parsec to kiloparsec scales in the region of knot C2. Deceleration does appear to occur at and beyond the sharp bend (knot C4), such that the flow might be only mildly relativistic by the end of the jet. The deceleration is accompanied by significant intensification of the magnetic field (see Table 1 and Jorstad & Marscher 2004). The latter follows the expectations of the model of Georganopoulos & Kazanas (2004), although the jump in field strength at the bend is about 4 times greater than the model predicts. This is in line with the supposition that a standing shock accompanies the bend in the flow. Homan et al. (2001) determined the apparent speed in the jet of the quasar 1222+216, $\beta_{\rm app} = (16.6 \pm 0.7)c$. The parsec scale jet (Fig. 4) aligns with the X-ray jet as well as with the inner part of the radio kiloparsec scale jet, which undergoes a sharp bend where the detected X-ray emission ends. The absence of X-ray emission beyond the apparent bend might be explained by deceleration of the jet flow due to intrinsic bending of the jet. Therefore, morphology and kinematics of the parsec-scale jet and structure of the X-ray jet support the high value of the bulk Lorentz factor on kiloparsec scales in the quasars 0827+243 and 1222+216.

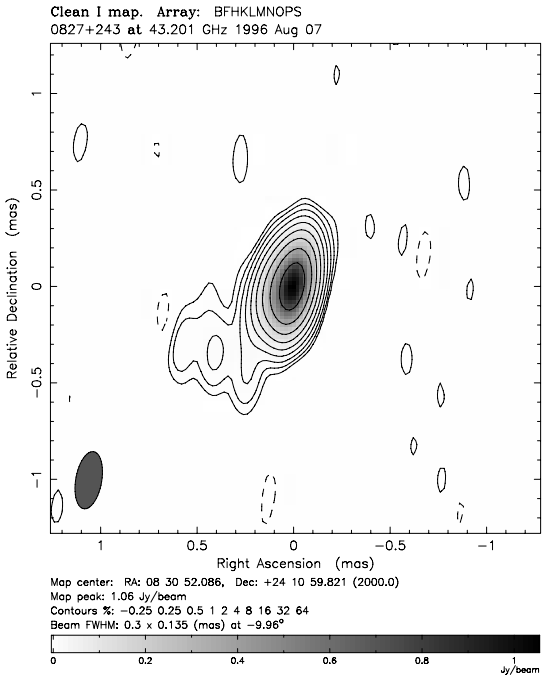

Fig. 3. VLBA image of the quasar 0827+243 from our program of monitoring a sample of γ-ray blazars with the VLBA by Jorstad et al. (2001).

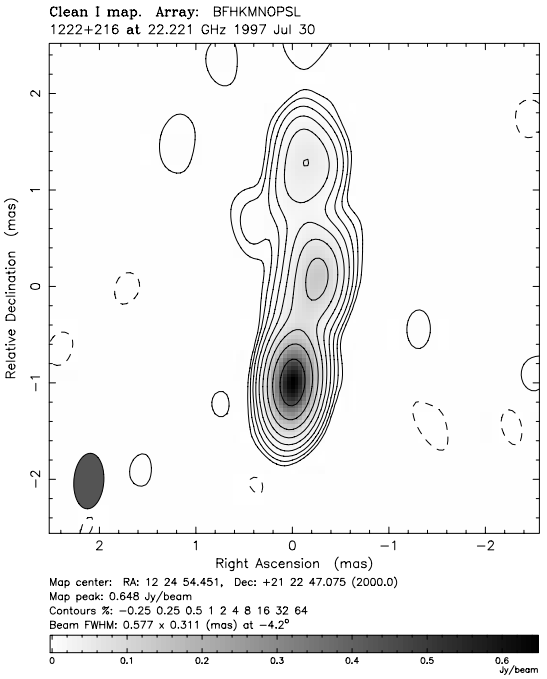

Fig. 4. VLBA image of the quasar 1222+216 from the same program.

The required kinetic luminosities of the X-ray emitting knots C4 and C in the quasars 0827+243 and 1317+520, respectively, are high, $\geq 10^{47}$ ergs s^{-1}, but perhaps possible for powerful jets. These values argue that the jet cannot be far from equipartition between the energy density of relativistic electrons and that of the magnetic field. Otherwise, the required luminosities would be excessive (see Dermer & Atoyan 2004). The derived kinetic luminosities of knots could also be reduced if the positively charged particles are mainly positrons or if there is a break in the electron energy distribution at Lorentz factor $\gamma \sim 2000$.

The characteristics of the knots allow more than one model for the spectral energy distributions of the jet features. The SEDs could arise from pure synchrotron emission from either a single or dual population of relativistic electrons Alternatively, the X-ray emission could result from inverse Compton scattering of the Cosmic Microwave Background photons by electrons with Lorentz factors as low as $\gamma \sim 15$. A test of these models might be obtained via deep imaging in the IR (with sensitivity $\sim$2 μJy) and in the optical (with sensitivity $\sim$10 nJy) regions at several bands for constructing the optical and IR spectral indices, and through detection the γ-ray emission from kiloparsec scale jets. Observations of the quasars 0827+243 and 1317+520 in the mid-IR region with the Spitzer Space Telescope are approved for Cycle 2, which we hope will detect the IR jets. If the IC/CMB model for the X-ray production in kiloparsec scale jets will be confirmed, future missions with sufficient angular resolution should detect large scale γ-ray jets.

Acknowledgements. This material is based upon work supported by the National Aeronautics and Space Administration under Chandra Guest Investigator grant no. GO2-3137X administered by the Smithsonian Astrophysical Observatory, and by the U.S. National Science Foundation under grant no. AST-0406865. The VLA and VLBA are facilities of the National Radio Astronomy Observatory, operated by Associated Universities Inc. under cooperative agreement with the National Science Foundation.

References

Celotti, A., Ghisellini, G., Chiaberge, M.: 2001, MNRAS 321, L1
Dermer, C.D., Atoyan, A.: 2002, ApJ 568, L81
Dermer, C.D., Atoyan, A.: 2004, ApJ 611, L9
Georganopolulos, M., Kazanas, D.: 2004, ApJ 604, L81
Homan, D.C., Ojha, R., Wardle, J.F.C.,Roberts, D.H., Aller, M.F., Aller, H.D., Hughes, P.A.: 2001, ApJ 549, 840
Jester, S., Röser, H.-J., Meisenheimer, K., Perley, R.: 2005, A&A 431, 477
Jorstad, S.G., Marscher, A.P., Mattox, J.R., Wehrle, A.E., Bloom, S.D., Yurchenko, A.V.: 2001, ApJS 134, 181
Jorstad, S.G., Marscher, A.P.: 2004, ApJ 614, 615
Marshall, H.L., Harris, D.E., Grimes, J.P., et al.: 2001, ApJ 549, L167
Marshall, H.L., Schwartz, D.A., Lovell, J.E.J., et al.: 2005, ApJS 156, 13
McNamara, B.R., Nulsen, P.E.J., Wise, M.W., Rafferty, D.A., Carilli, C., Sarazin, C.L., Blanton, E.L.: 2005, Nature 433, 45
Piner, B.G., Bhattarai, D., Edwards, P.G., Jones, D.L.: 2005, BAAS 110, 14
Sambruna, R.M., Gambill, J.K., Maraschi, L., Tavecchio, F., Cerutti, R., Cheung, C.C., Urry, C.M., Chartas, G.: 2004, ApJ 608, 698
Schwartz, D.A., Marshall, H.L., Lovell, J.E.J., et al.: 2000, ApJ 540, L69
Siemiginowska, A., Bechtold, J., Aldcroft, T.L., Elvis, M., Harris, D.E., Dobrzycki, A.: 2002, ApJ 570, 543
Tavecchio, F., Maraschi, L., Sambruna, R.M., Urry, C.M.: 2000, ApJ 544, L23